THE JOURNAL OF PHYSICAL CHEMISTRY C

ARTICLE

pubs.acs.org/JPCC

Synthesis of Inorganic Tubes under Actively Controlled Growth Velocities and Injection Rates

Rabih Makki and Oliver Steinbock*

Department of Chemistry and Biochemistry, Florida State University, Tallahassee, Florida 32306-4390, United States

Supporting Information

ABSTRACT: We describe an experiment that establishes control over the growth velocities of macroscopic tubes in the reaction between a polymerizable inorganic anion and a nonalkali metal ion. Our approach is demonstrated for the injection of an acidic cupric sulfate solution into a large volume of a basic sodium silicate solution. The forming tube is pinned to a gas bubble that is held at the end of a hollow glass rod. The tube's linear growth follows the speed of the glass rod (0.5−11 mm/s), while its radius (0.2−1.6 mm) is self-selected according to the volume conservation of the injected solution. Depending on the experimental conditions, tube growth occurs at either the moving gas bubble or the stationary glass capillary. Oscillatory modulations of the growth velocity provoke the formation of hollow nodules on the outer tube surface. These nodules form after each rapid velocity decrease at exponentially decaying rates and seem to be energetically favored over a sudden isotropic increase in tube radius.

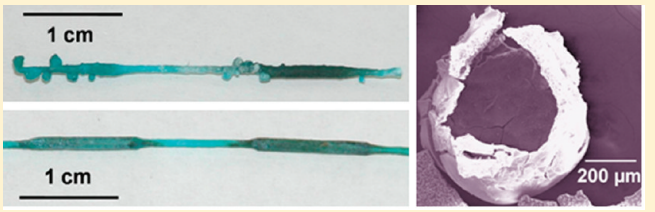

INTRODUCTION

Externally controlled self-assembly and self-organization can produce a broad spectrum of hierarchically ordered structures and materials.[1] Examples include three-dimensional objects such as nanoparticle assemblies,[2,3] solid and hollow spheres,[4] helices,[5] fibers,[6] rods,[7] and tubes of large aspect ratio.[8−10] Because molecular and supramolecular self-assembly occurs close to thermodynamic equilibrium, its approximate outcome is typically easier to anticipate than the results of self-organizing processes that require conditions far from equilibrium.[11−17] This design advantage of self-assembly comes at the price of comparably low temporal and spatial complexity which for self-organization can be tremendously large.[18,19] The exploration of these (nonexclusive) processes is of great interest to materials science. Its key challenges, however, are centered in the realm of physical chemistry.

The formation of macroscopic, inorganic tubes is an important example for this unconventional approach toward materials synthesis and device production. Several groups have used template-directed sol−gel methods to control the shape of the forming tubes.[20] Nakamura and Matsui prepared rhomboidal nanotubes by hydrolyzing tetraethyl orthosilicate in a mixture of ethanol, water, ammonium hydroxide, and racemic tartaric acid.[21,22] The underlying mechanism involves the deposition of amorphous silica around crystals of ammonium DL-tartrate that grow in reacting solutions of tartaric acid and ammonium hydroxide.[23,24] Another approach has been pursued by Cronin and co-workers[25] who reported the spontaneous formation of hollow tubes in an aqueous system containing an organic cation and polyoxometalate crystals. The diameter of these tubes varies in the range of several micrometers, and their length can reach up to a few millimeters. Moreover, directional control was achieved during synthesis by applying external concentration gradients and electric fields.[26]

Inorganic tubes also form during the reaction of aqueous silicate, carbonate, borate, and phosphate solutions with (nonalkali) metal ions in salt crystals, pellets, or gel beads.[8,27−30] This chemistry is closely related to the processes in "silica gardens" which are a well-known demonstration experiment in chemical education but also attract modern research interest.[31−33] Tubes grow usually upward and are, in the simplest case, templated around a buoyant jet of metal salt solution. This reactive jet is driven by a self-organized osmotic pump at the base of the structure. The typical tube radii are in the range of tens of micrometers to single millimeters. Many studies have focused on the characterization of the resulting tube materials and the exploration of potential applications. For instance, Collins et al. studied the morphology of the aluminosilicate tubes and revealed the presence of nano- to micrometer hierarchical structures.[34] Subsequent analyses by the same group showed that the tubes are also highly efficient Brønsted acid catalysts.[35,36]

In the latter type of systems, tubular structures can also be produced by externally controlled hydrodynamic delivery.[37,38] This approach typically involves the steady injection of aqueous solutions of nonalkali metal ions into solutions containing one of the anions mentioned above. Examples include the preparation of photocatalytically active, photoluminescent ZnO/SiO_2 tubes[39] and demonstrations of $Cu(OH)_2/SiO_2$ tubes as microfluidic conduits.[37] This injection method also allowed for the identification of three distinct growth regimes (jetting, popping, and budding), which occur for different ranges of density differences between the two reactant

Received: May 19, 2011
Revised: July 25, 2011
Published: July 26, 2011

dx.doi.org/10.1021/jp2046849 | J. Phys. Chem. C 2011, 115, 17046–17053

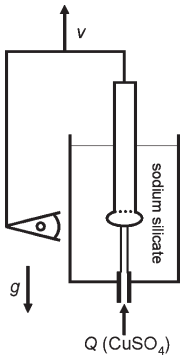

Figure 1. Schematic representation of the experimental setup. A computer-controlled motor moves a gas-filled glass rod and a video camera upward with speed *v*. Attached to the bottom end of the glass rod is a large gas bubble. Simultaneously, copper sulfate solution is injected into a large reservoir of silicate solution at a constant pump rate *Q*. The vector *g* denotes gravity.

solutions. The radius of the forming tubes increases with increasing flow rate and concentration of the injected solution.[40]

Additional control of the growth process is achieved by templating the tube with a buoyant gas bubble. The bubble is pinned to the upper end of the upward growing tube and held in this wall-forming reaction zone by interfacial tension. Quantitative measurements by Thouvenel-Romans et al.[41] revealed that the radius of such tubes is tightly controlled by the radius of the guiding bubble. For the investigated parameter range, the radius ratio (tube-to-bubble) varies systematically between 0.8 and 0.95. Moreover, the bubble-guided tubes select their growth velocity according to the volume conservation of the injected solution.[41]

In this article, we present and utilize an experimental technique in which similar macroscopic tubes form not under radius-templating conditions but under strict control of the tubes' linear growth velocity. This novel constraint is introduced by pinning the forming tube to a motorized glass rod. We also investigate the response of the system to controlled velocity oscillations and describe unexpected dynamics that form hollow, nodular structures on the tube.

EXPERIMENTAL SECTION

A schematic representation of our setup is shown in Figure 1. It involves the hydrodynamic injection of a 0.50 M cupric sulfate solution ($CuSO_4.5H_2O$, Spectrum) into a large reservoir containing a 1.0 M sodium silicate solution ($Na_2SiO_3.5H_2O$, Fisher) at 22 ± 1 °C. All chemicals are of analytical grade, and solutions are prepared using nanopure water (18 MΩ cm, Easy-pure UV, Barnstead). Injection is carried out through a vertical glass capillary (length = 27 mm, inner diameter ≈1.1 mm) into a cylindrical glass vessel (height ≈90 mm, inner diameter = 32 mm) containing the sodium silicate solution. The flow rate of the injected cupric sulfate solution is controlled by a syringe pump (KD Scientific 200) and varied between 1−25 mL/h, while the concentrations of the two solutions are kept constant. A hollow glass rod (length = 24 cm, inner diameter = 4.0 mm) is centered in the middle of the glass vessel and positioned 3−5 mm above the glass capillary. The glass rod is connected to an air-filled syringe which is used to manually create a large air bubble at the lower end of the glass tube. Once a tube starts to grow, it is pinned to the glass tube through this cushion-like gas interface. The glass rod moves up vertically at a definite speed forming a nearly straight tube in its wake. A charge-coupled device camera (COHU 2122) is mechanically connected to the glass rod, and both components move together in vertical direction. The speed of this assembly is controlled by a servo motor/controller system (BLM-N23-50-1000-B, CDS-3310, Galil) and varied in the range of 0.5−12.0 mm/s. The camera signal is digitized at a rate of 1−4 frames/s by a frame grabber board (DT 3155, Data Translation) and HL Image ++97 software. For additional characterization, the product structures are removed from the silicate solution, washed three to four times with water, and dried overnight under ambient conditions. The specimens are then placed in a vacuum desiccator to remove the remaining moisture and finally gold-sputtered to enhance the conductivity of their surface. Scanning electron microscope (SEM) images are obtained on a JEOL JSM-5900 instrument at an acceleration voltage of typically 30 kV.

RESULTS

In numerous initial experiments, we attempted to pin the upward growing tubes to upward moving solid objects of various diameters (1−10 mm) and shapes, including solid rods with flat, cone-shaped, and half-spherical tips. Also, several materials were tested such as Teflon, stainless steel, borosilicate glass, and plexiglass. These experiments did not yield the desired direct contact between the growing tube rim and the moving obstacles. More specifically, we found either no pinning at all or pinning occurring between the growth zone and a solid product "plug" that tightly adhered to the tip but had no reproducible shape. These plugs had vertical lengths of not more than a few millimeters and formed during the first second of the growth process.

The problem of achieving a more direct contact between the externally controlled pinning site and the forming tube can be solved by the introduction of a gas bubble (here, air) that effectively serves as a soft cushion, prevents permanent adhesion, and in the future might be used for doping purposes. These bubbles are generated at the bottom end of a hollow glass rod where they are reliably held by interfacial tension. Because of the decreasing hydrostatic pressure in the silicate solution, they expand slightly during the upward motion of the anchoring glass rod. The bubble radius is usually 5−10 times bigger than the radius of the forming tube to avoid any direct contact between the product material and the outer surface of the glass rod. Within the size range studied, the radius of the air bubble has little or no effect on the radius of the forming tubes (results not shown). Notice that this behavior is qualitatively different from the bubble-templated growth discussed in earlier studies,[39,41] which did not involve an external control of the linear growth velocity. After pinning, the glass tube moves vertically up according to a predetermined speed curve.

We first discuss the case of constant rod speeds. Under these conditions, we find that the growth velocity of the forming tube is identical to the rod speed. Furthermore, the hollow product structure continues to grow all the way to the silicate−air interface where the gas bubble vanishes. We did not investigate the subsequent horizontal growth at the solution−air interface but usually stopped the injection of copper sulfate solution when the lower rod end exited the silicate reservoir. During the entire reaction process, the bubble remains attached to both the growing tube and the moving glass rod. Furthermore, we observe no lateral movement. If the pump is stopped before the tube reaches the silicate−air interface, linear growth ceases instantaneously. For the

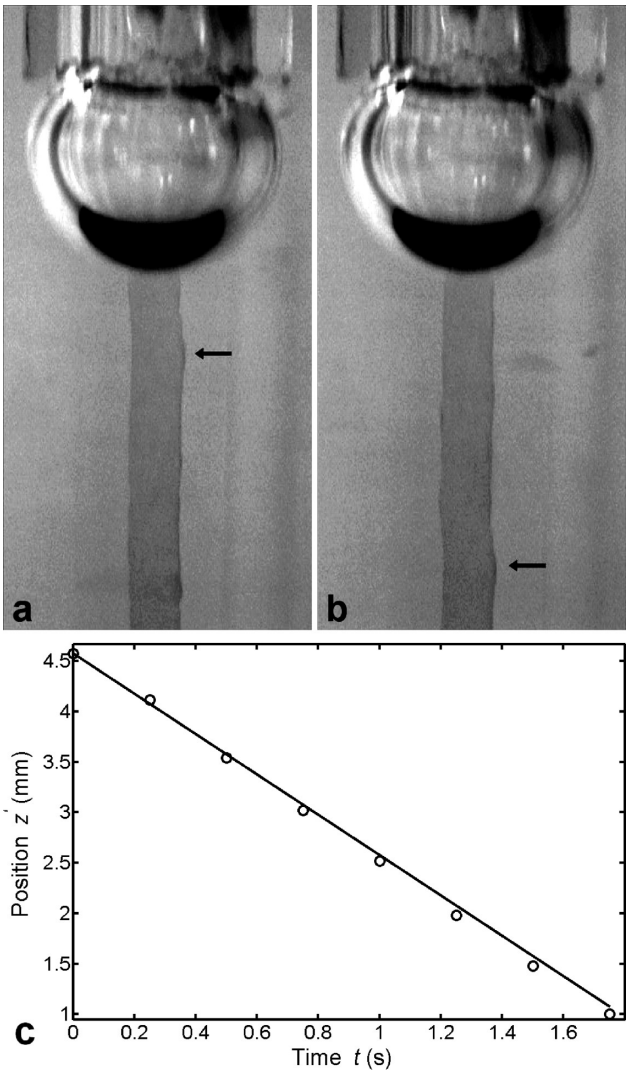

Figure 2. Tube formation in close vicinity of the air bubble. (a,b) Snapshots recorded from a camera in the comoving reference frame of the bubble. The time interval between the two frames is 1.75 s. Black arrows mark the position of a small wall deformation. Field of view: $7.3 \times 14.9\ mm^2$. (c) Motion of the deformation in the reference frame of the bubble. Open circles denote the measured positions. The solid line is the linear dependence $z' = -2\ mm/s\ t + z_0$ expected for an object that is stationary in the laboratory frame of reference. The flow rate of the injected cupric sulfate solution is 5 mL/h, and the velocity of the glass tube is 2 mm/s.

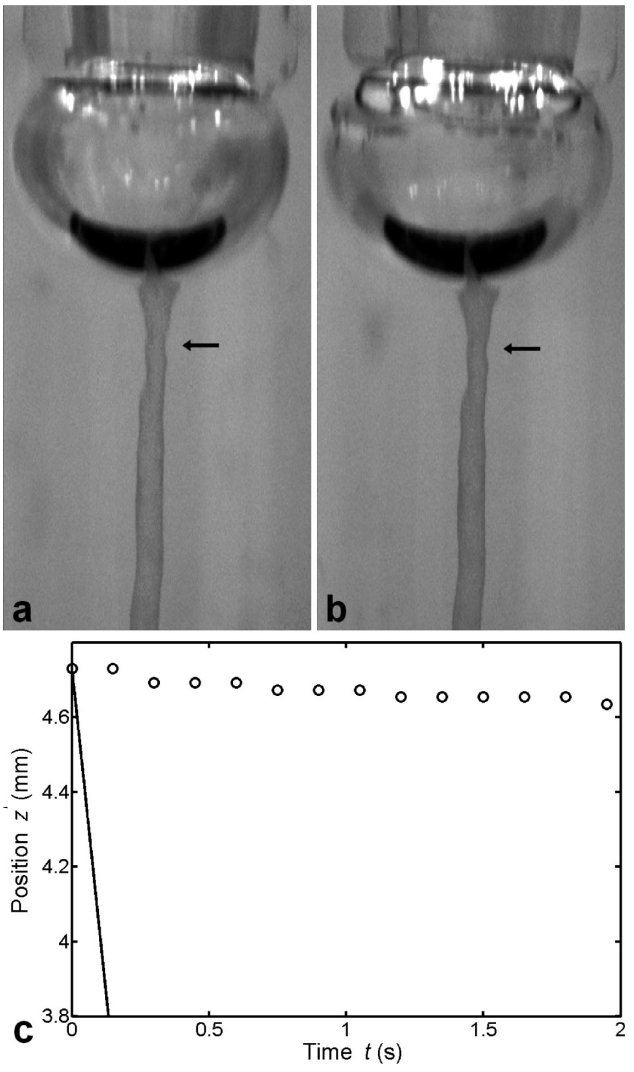

Figure 3. Tube formation in close vicinity of the injection nozzle. (a,b) Snapshots recorded from a camera in the comoving reference frame of the bubble. The time interval between the two frames is 2 s. Black arrows mark the position of a small feature on the tube wall. Field of view: $7.3 \times 14.9\ mm^2$. (c) Motion of the deformation in the reference frame of the bubble. Open circles denote the measured positions. The solid line is the linear dependence $z' = -7\ mm/s\ t + z_0$ expected for an object that is stationary in the laboratory frame of reference. The flow rate of the injected cupric sulfate solution is 5 mL/h, and the velocity of the glass tube is 7 mm/s.

experimental parameter space investigated, the velocity-controlled tubes are nearly straight and have outer radii in the range of 0.2−1.6 mm. However, our method should also allow the production of thinner and wider tubes. The tube length is limited by the height of the silicate reservoir.

To our knowledge, all prior studies on the formation of precipitation tubes found that with respect to the injection nozzle or seed crystal, longitudinal growth occurs only at the far end of the tube.[8,41] For upward growing structures, this implies that vertical growth occurs only at the upper rim of the structure. In our study, however, the location of the growth zone depends on the experimental conditions and is found either at the air bubble or at the tube's lower end (i.e., close to the solution-delivering glass capillary). Figure 2 shows data from a representative experiment in which new wall material is produced directly underneath the air bubble. The image frame b is recorded 1.75 s after frame a. Both images reveal a small convex deformation on the wall of the tube (see black arrows). Its distance to the bubble in Figure 2b is larger than that in Figure 2a. Notice that our image data are recorded in a reference frame that moves with the speed of the glass rod. Consequently, new tube material must have formed in close vicinity to the bubble. This conclusion is quantified in Figure 2c where the vertical position z' of the deformation in the comoving coordinate system is plotted as a function of time. The experimental data (open circles) are well described by a linear function of a slope of −2 mm/s. This speed is identical to the externally controlled rod velocity. Accordingly, the wall deformation is stationary in the laboratory frame of reference.

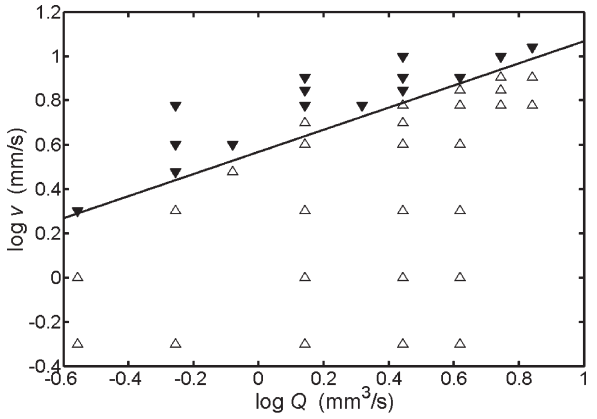

Figure 4. Phase diagram of the growth position in terms of the volume flow rate Q and the rod speed v. Open triangles indicate growth at the air bubble, while solid triangles mark conditions for which tube growth occurs close to the glass capillary. The straight line estimates the critical velocity between the two growth regimes as $\log [v/(1\ \mathrm{mm/s})] = 0.5 \times \log [Q/(1\ \mathrm{mm}^3/\mathrm{s})] + 0.567$.

Figure 3a,b shows images of a representative example in which tube growth occurs close to the injection nozzle. As in Figure 2, we mark a small deformation on the wall of the forming tube and track it with black arrows. In the reference frame of the bubble, the vertical position of the deformation is stationary, and in the laboratory frame, it must hence move upward with the speed of the pinning glass rod. This finding shows that the growth zone cannot be close to the air bubble. This conclusion is also confirmed by Figure 3c, which shows that the vertical position z' of the deformation is nearly stationary in the reference of the bubble. The small decrease in the measured z' values is due to a hydrostatic pressure induced expansion of the air bubble. The latter effect is rather small but can be discerned by comparing Figure 3a and b. In Figure 3c, we also graph the linear curve expected for stationary objects in the laboratory frame. This dependence is clearly not in agreement with our data. Additional evidence for the existence of tube growth close to the injection point is also obtained from experiments in which a stationary camera monitored the area above the nozzle (not shown).

To better understand and control the observed changes in the tube growth position, we carried out experiments in which the rod speed, v, and the flow rate, Q, were varied systematically. Each measurement (i.e., at a given v and Q) was repeated three to four times. The highly reproducible results are summarized in Figure 4. Open triangles pointing upward represent experimental conditions for which growth occurs at the air bubble, while solid triangles pointing downward indicate growth near the glass capillary. The data show that growth at the bubble is associated with high flow rates and small velocities. In addition, the data suggest the existence of a critical velocity, v_{crit}, above which growth always occurs in close vicinity to the glass capillary. For our experimental conditions and over the relatively small range of flow rates studied (1−25 mL/h), this critical velocity is well described by a power law of the form

$$v_{crit} = kQ^{1/2} \tag{1}$$

where the proportionality constant is $k = 3.7\ (\mathrm{mm\ s})^{-1/2}$.

Earlier studies on tube formation in aqueous silicate/metal ion systems revealed two qualitatively different types of growth dynamics:[28,29,40] (i) "closed growth" for which the injection rate

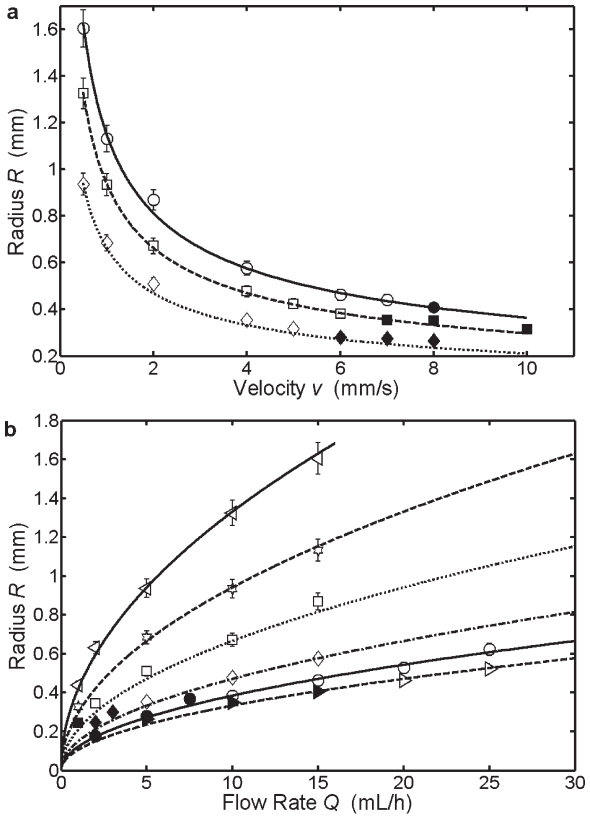

Figure 5. Average tube radius as a function of the externally controlled physical parameters, v and Q. (a) Tube radius as a function of glass rod velocity for three different flow rates: $Q = 5$ mL/h (diamonds), 10 mL/h (squares), and 15 mL/h (circles). (b) Tube radius as a function of flow rate for six different glass tube velocities: $v = 0.5$ mm/s (leftward pointing triangles), 1 mm/s (stars), 2 mm/s (squares), 4 mm/s (diamonds), 6 mm/s (circles), and 8 mm/s (rightward pointing triangles). Open markers denote conditions for which growth occurs at the air bubble, while solid markers indicate growth at the injection nozzle. The continuous curves show the function $R = (Q/(\pi v))$, which assumes that the injection rate equals the growth rate of the enclosed tube volume.

equals (within the experimental error) the volume increase of the hollow tube structure and (ii) "open growth" for which tube formation occurs at a much slower rate than the volume flow rate Q. A characteristic example for the latter scenario is the templating of a tube around a reactive jet of salt solution ("jetting growth"). Measurements on bubble-templated growth, however, revealed strong evidence for volume conservation.[41]

We find that the externally controlled tube formation discussed here belongs to the class of "closed growth" processes. Figure 5a,b shows measurements of the tube radius R that support this statement. In Figure 5a we plot, for three different flow rates, the radius as a function of the rod speed. Clearly, the tube radius decreases with increasing speed. The data in Figure 5b further reveal that the radius increases with increasing flow rate. Both figures also show the curves expected under strict volume conservation as shown in the equation below.

$$Q = \pi R^2 v \tag{2}$$

The previous equation assumes that the volume flow rate $Q = \mathrm{d}V/\mathrm{d}t$ of the injected solution is identical to the change in enclosed tube volume $\pi R^2\, \mathrm{d}h/\mathrm{d}t = \pi R^2 v$, where t and h denote

dx.doi.org/10.1021/jp2046849 |J. Phys. Chem. C 2011, 115, 17046–17053

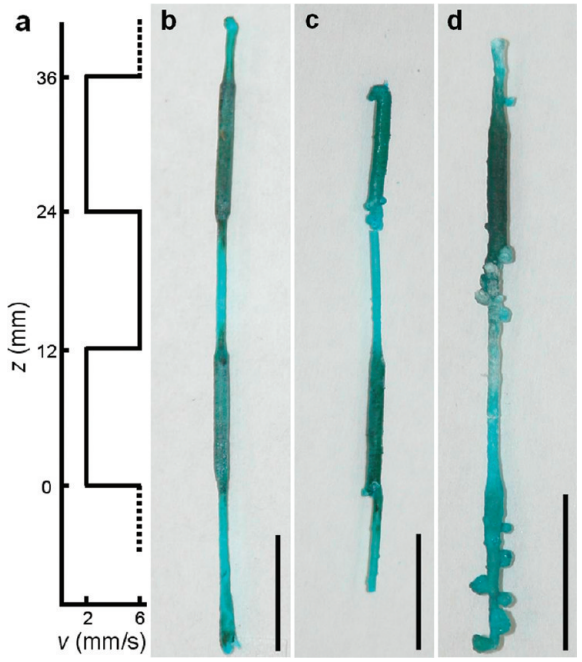

Figure 6. Tube growth under externally controlled oscillations of the linear growth velocity. (a) Velocity of the pinning glass rod as a function of height z in the reaction container. (b−d) Three representative dried samples obtained under these nonstationary growth conditions. The tubes in frames b and c are shown at the same length scale as the velocity profile in frame a. Scale bars: 1 cm.

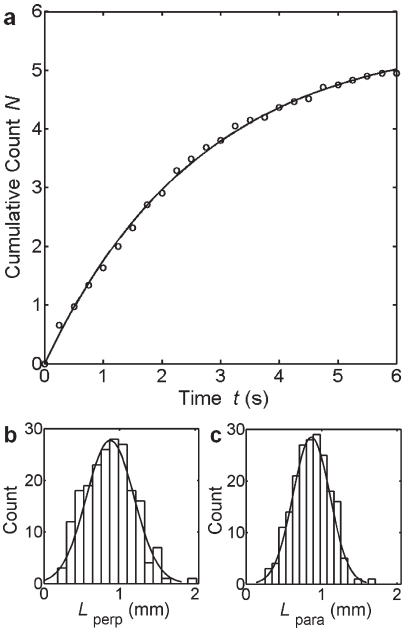

Figure 7. (a) Dynamics of nodule formation in response to a sudden velocity decrease from 6 to 2 mm/s at time $t = 0$. Open circles represent the cumulative number of detected nodules per oscillation cycle obtained from numerous experiments. The solid curve is the best exponential fit. (b,c) Distributions of the nodule length perpendicular (b) and parallel (c) to the tube. The solid lines are the best fitting normal distributions. Flow rate: $Q = 10$ mL/h.

time and tube height, respectively. The experimental data are in excellent agreement with this simple expression. In addition, Figure 5 distinguishes between tube growth at the bubble (open symbols) and in close vicinity to the injection nozzle (solid markers). Both growth scenarios obey the discussed volume conservation.

So far, the velocity of the pinning glass rod was kept constant in each experiment. However, our setup readily allows the exploration of tube formation for nonsteady rod motion and/or pump rates. Next, we discuss the case of oscillating velocities and constant flow rates as a simple but interesting example.

Figure 6 shows three representative samples synthesized under such conditions. The optical micrographs depict the samples after washing and drying. During synthesis, the rod velocity was alternated between 2 and 6 mm/s, while the flow rate was kept constant at 10 mL/h. Under these conditions, growth always occurs at the air bubble (compare to Figure 4). We maintained the low and high velocity phases for different time intervals so that the glass rod traveled equal distances during the alternating phases. For the samples in Figure 6, the low velocity was maintained for 6 s, while the high velocity was held for 2 s. Accordingly, the rod moves 12 mm (6 s × 2 mm/s and 2 s × 6 mm/s) during each velocity phase. The total repeat period of the cycle is 8 s during which the glass rod is lifted up by 24 mm. Figure 6a shows this velocity profile in terms of the vertical height z (laboratory frame of reference). The samples in Figure 6b,c are shown to the same scale, while Figure 6d has a slightly higher magnification.

The three tube samples in Figure 6 reveal systematic variations of the diameter between approximately 0.38 mm and 0.66 mm. These thin and thick regions each have a length of approximately 12 mm, which is the expected value based on the aforementioned discussion. The first two samples (b,c) are lined-up with the velocity profile in frame a according to the expected thick/slow and thin/fast dependence (see Figure 5).

We re-emphasize that our discussion of tube thickness refers to the radius of the hollow, cylindrical structure and not to the width of the tube wall. Preliminary data from scanning electron microscopy does not reveal any evidence for a strong dependence of the wall width on the growth velocity. Unfortunately, this interesting analysis is severely hindered by local variations and the very rough and morphologically complex structure of the interior tube surface. Typical SEM images are shown in the Supporting Information (Figure 1S). These micrographs suggest that for the conditions analyzed here, velocity-dependent variations in wall thickness are small or nonexistent.

Nonetheless, we observe striking color differences between the thin and thick regions of the samples in Figure 6. Clearly, the wide regions have a darker (often nearly black) color, while the thin regions are bright blue or greenish blue. Although at this point we cannot fully rule out effects caused by variations in the wall thickness, this color difference is probably indicative of chemical differences. For instance, it is possible that copper(II) oxide causes the dark appearance of the wide tube regions. Clearly, direct spectroscopic evidence is needed to identify the origin of the observed differences.

The tube in Figure 6d shows an additional feature that is absent in sample b and comparably weak in c. Attached to the outer tube wall are numerous nodules. These structures can be detected already during the growth process and form along with the new wall material in close vicinity to the bubble. Nodules form predominantly during the transition from fast (thin tube segments) to slow growth (thick segments). However, occasionally they can also be observed in the reverse transition and even during steady growth but then at greatly reduced frequencies.

Figure 7 provides additional information on the dynamics of nodule formation. For this statistical analysis, we measure from optical data the time t at which a nodule forms. The time $t = 0$ is the instant at which the glass rod shifts from fast to slow speed. This analysis is repeated for 50 oscillation cycles (different samples) and yields the cumulative histogram in Figure 7a. Open circles represent the cumulative number of nodules N obtained per oscillation cycle. The data show that a sudden drop in the velocity of the pinning glass rod causes, on average, the formation of five to six nodules. The rate of nodule formation is relatively high immediately after the velocity drop but then decays smoothly to zero. These dynamics are well described by an exponential function of the form

$$N(t) = N_\infty(1 - e^{-t/\tau}) \quad (3)$$

with a saturation value of $N_\infty = 5.6$ and a relaxation time of $\tau = 2.6$ s.

Notice that the half of the tube facing away from the camera is not detected in these experiments. Any nodules forming on that side do not enter into our analysis. The presented data does not contain any corrections for this detection problem. One can assume that these missed nodules account for approximately half of all nodules.

We interpret this relaxation process as a pressure-induced instability of the upward moving, ring-shaped reaction zone. During the fast velocity drop, the pressure difference across the tube wall increases rapidly as the new reactant solution is delivered. The symmetry-preserving response of the wall-forming reaction zone would be to isotropically increase its radius. However, this nodule-free behavior is rarely observed. Our evidence suggests that it is energetically favorable for the reaction zone to produce a single breach site that, like a relief valve, swiftly compensates for the increasing pressure. Because of the reactive character of the interior and exterior solutions, this site nucleates an expanding nodule. However, the system cannot accomplish lasting pressure compensation with a single nodule as shown by the sequential formation of an average of 5.6 detected nodules per velocity drop. This finding suggests that the membrane-like wall of the newly formed nodule changes its elastic characteristics during its short growth process. After ~1 s of growth, these changes allow for the nucleation of a new (and hence softer) nodule which then terminates the growth of the earlier nodule. Simultaneously, the tube radius relaxes toward its new steady-state value, which causes the observed decrease in the rate of nodule formation.

Sudden velocity *increases* are associated with a pressure decrease in the tube's interior. This situation does not favor the formation of nodules as illustrated by the samples in Figure 6, which reveal not more than two nodules over the total of six segments formed under increasing velocities. Under these conditions, the upward growing tube decreases its radius in a continuous and often nearly isotropic fashion. Visual inspection of numerous samples (see Figure 6 for examples) suggests that the radius decreases much slower than the essentially instantaneous change in velocity. This result shows that the nodule instability is not symmetric with respect to positive and negative pressure differences across the wall. Moreover, it could involve the stretching of the deformable top portion of the tube. We briefly mention that similar instabilities exist in certain mechanical systems. For instance, if one inflates several connected and nearly identical rubber balloons, they will not expand simultaneously but sequentially.[42] This instability is caused by the nonmonotonic pressure−volume curve of the rubber membrane, which is known to everyone as the subjective experience that balloons are difficult to inflate at small volume. However, deflating balloons are not affected by this instability, and connected balloons decrease their volume in synchrony.[42]

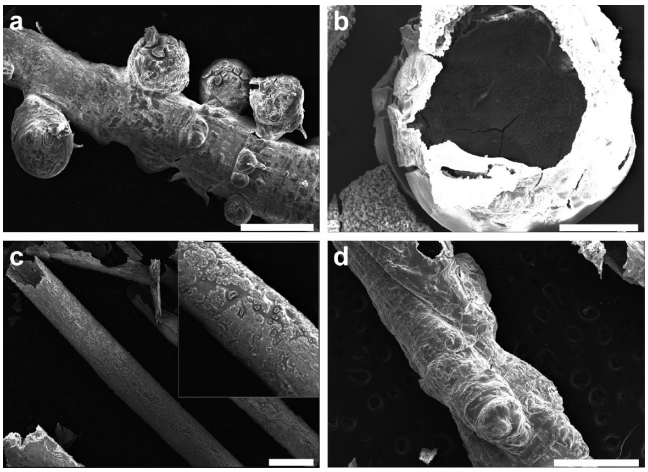

Figure 8. Scanning electron micrographs of tubes and nodules. (a) Tube segment formed immediately after a transition to a lower rod velocity. Several nodules are attached to the tube. (b) Close-up view of a nodule that broke postsynthesis. The structure is clearly hollow. (c) Tubes formed for conditions that induce growth in close vicinity of the injection nozzle. Flow rate: 20 mL/h. Rod velocity: 10 mm/s. (d) A tube fragment with a folded, helical morphology. Flow rate: 2 mL/h. Rod velocity: 0.5 mm/s. Scale bars: (a,c,d) 1 mm and (b) 0.2 mm.

While all nodules are hollow and of an overall round shape, their size shows some variation. We have analyzed optical micrographs of around 200 nodules and measured their length perpendicular, L_{perp}, and parallel, L_{para}, to the tubes' long axis. The distribution of these data is shown in Figure 7b,c. The histograms reveal that both L_{perp} and L_{para} are well described by normal distributions. The mean values are 0.87 and 0.86 mm, respectively. These averages show no dependence on the time, t, measured from the moment of the velocity drop (see Figure 2S in the Supporting Information). Under the assumption of a spherical shape, they correspond to an average volume of 0.34 mm^3 per nodule. The standard deviations of the L_{perp} and L_{para} distributions are 0.31 and 0.24 mm, respectively.

The average nodule volume of $V_b = 0.34$ mm^3 allows us to discuss the initial rate of nodule formation in Figure 6a. If we assume that the initial response of the system consists solely of nodule formation (i.e., constant radius), then volume conservation yields a simple equation for the initial rate, dN/dt:

$$\frac{dN}{dt} = \frac{v_f - v_s}{v_f}\frac{Q}{V_b} \quad (4)$$

where v_f and v_s denote the fast and slow rod speed, respectively. For the analyzed experiments the latter equation yields 5.4 s^{-1}. The initial rate of nodule formation can also be measured from the slope of the exponential fit in Figure 7a, which equals 2.1 s^{-1} or 4.2 s^{-1} if we correct for undetected nodules on the back of the tube. Consequently, there is good agreement between our experimental data and the suggested analysis.

All hollow tubes obtained under external velocity control are sturdy enough to withstand washing, drying, and postsynthesis modifications. It is therefore possible to inspect their morphologies

using a techniques such as scanning electron microscopy (SEM). Figure 8a shows a representative micrograph of a tube segment formed in the wake of a velocity drop. Attached to the tube are four nodules. On the basis of the data in the histograms in Figure 7b,c, their size falls within a high-probability interval. The tube surfaces also show some smaller nodular features, which would have remained undetected during the optical monitoring of the growth experiment. If related to the velocity perturbation, their presence might explain the small (20%) deviation between the expected and measured initial rates of nodule formation. They could further suggest that not every breach induces the formation of a "mature" millimeter-size nodule. In addition, Figure 8b shows a top view of a broken nodule. The SEM micrograph supports our earlier statement that these structures are hollow. The surface of the nodules is rather rugged. The crack-like features in the outer (silica-rich) layer are likely caused by the drying process.

Figure 8c provides a detailed view of a tube formed under conditions that induce growth close to the injection nozzle. The structure is clearly hollow. Notice that the latter observation is nontrivial. While growth at the bubble requires that the cupric sulfate solution passes through the entire tube, growth at the nozzle does not depend on such a transport conduit; the solid product is formed and then simply pushed upward. Consequently, this product could have taken the form of a solid rod, which is clearly ruled out by our observations. The micrograph also shows that the tube is very straight and has, by comparison with the other micrographs, a fairly smooth outer surface.

Lastly, Figure 8d depicts a tube fragment with a twisting, helical morphology. This shape is occasionally observed under conditions of low flow rates (here 2 mL/h) and forms during the growth process. Usually this type of tube grows upward for a few millimeters with the expected cylindrical geometry. Then, it collapses to a helical ribbon but stays pinned to the bubble and grows upward in a twisting fashion. This observation reveals that fluid flow through the helical structure is possible. Notice that related structures have been observed in an earlier study on tube formation, in which the motion of the pinning gas bubble was not externally controlled.[41]

DISCUSSION

In summary, we have established a new method for the production and study of millimeter-scale inorganic tubes with tightly controlled radii and lengths. Our approach complements recently developed flow-injection methodologies by pinning the forming tube through a gas interface to a moving glass rod with a predetermined speed. Under these conditions of constant volume flow rates and constant growth velocities, the tubes select their radius in a way that conserves the volume of the injected solution.

In principle, length-extending tube growth can be imagined to occur at any single position or any arbitrary interval(s) along the precipitation structure. To our knowledge, however, all earlier studies reported that with respect to the reactant source (e.g., the injection point or seed particle) this process occurs at the *distant* tube end (see, e.g., refs 8 and 41). For the conventional case of upward growing tubes, this implies vertical growth at the top end of the tube. Surprisingly, our study reveals that this key process can also occur at the bottom (Figure 3). Under such conditions, the entire tube is pushed upward by the production of new wall material at the structure's base. Here, this motion is assisted by the moving bubble to which the tube's upper end is pinned via interfacial forces.

This novel result raises the question of the stability of the reaction zone's location (and width) along the tube axis. Notice that for reactant delivery from the bottom, this position cannot move downward into the already solidified (and mechanically supported) tube region. Accordingly, the likely scenarios are (i) a stationary reaction zone and (ii) an upward moving reaction zone. Both cases have been observed in our study (see Figures 2−4). The vertical motion of the reaction zone depends on a variety of factors that affect the precipitation rate, in particular the reactant concentration within the tube and the transport of the exterior reactant through the membrane-like interface. The concentration of the interior reactant is expected to decrease with increasing distance from the source. This effect should be strongest in the growth zone. Accordingly, a similar dependence should exist for the reaction rate. The influx of exterior reactant, however, is faster at the top of the forming tube where the two solutions are essentially in direct contact and not separated by a colloidal membrane, gel-like layer, or solid wall. The interplay of these two, opposing factors might be the source of the observed change between "top" and "bottom" growth. Clearly, more experimental data and theoretical analyses are needed to understand this interesting feature.

The second unexpected result of this study concerns the formation of hollow nodules in response to a sudden decrease in the pinning bubble/rod velocity. As we have already mentioned, this process reveals a second instability of the forming tube capable of breaking the cylindrical symmetry of the precipitation structure. At its heart are the visco-elastic and mechanical characteristics of the forming membrane that dictate whether a local breach is favored over a global stretch of the tube's top portion. Further systematic measurements of the tube dynamics in response to velocity jumps might provide additional insights into this important aspect. A related and highly interesting question is why the observed nodules fail to become secondary tubes. Currently, we cannot rule out the existence of experimental conditions under which such branching events occur. If velocity variations induce tube branching, our method would also add a very useful design feature to the production of hollow, inorganic conduits.

ASSOCIATED CONTENT

Supporting Information. Representative movies of the main growth dynamics, SEM micrographs of the cross-section of the tube wall, and additional data on the nodule size. This material is available free of charge via the Internet at http://pubs.acs.org.

AUTHOR INFORMATION

Corresponding Author
*E-mail: steinbck@chem.fsu.edu.

ACKNOWLEDGMENT

This material is based upon work supported by the National Science Foundation under Grant No. 1005861. We thank Dr. Eric Lochner for assistance.

REFERENCES

(1) Mann, S.; Ozin, G. A. *Nature* **1996**, *382*, 313.

(2) García-Ruiz, J. M.; Melero-García, E.; Hyde, S. T. *Science* **2009**, *323*, 362.
(3) Murray, C. B.; Kagan, C. R.; Bawendi, M. G. *Annu. Rev. Mater. Sci.* **2000**, *30*, 545.
(4) Chen, M.; Wu, L.; Zhou, S.; You, B. *Adv. Mater.* **2006**, *18*, 801.
(5) Delclos, T.; Aimé, C.; Pouget, E.; Brizard, A.; Huc, I.; Delville, M.-H.; Oda, R. *Nano Lett.* **2008**, *8*, 1929.
(6) Kubo, S.; Kosuge, K. *Langmuir* **2007**, *23*, 11761.
(7) Kuijk, A.; van Blaaderen, A.; Imhof, A. *J. Am. Chem. Soc.* **2011**, *133*, 2346.
(8) Makki, R.; Al-Humiari, M.; Dutta, S.; Steinbock, O. *Angew. Chem., Int. Ed.* **2009**, *48*, 8752.
(9) Patzke, G. R.; Krumeich, F.; Nesper, R. *Angew. Chem., Int. Ed.* **2002**, *41*, 2446.
(10) Rao, C. N. R.; Govindaraj, A. *Adv. Mater.* **2009**, *21*, 4208.
(11) Corliss, J. B.; Dymond, J.; Gordon, L. I.; Edmond, J. M.; von Herzen, R. P.; Ballard, R. D.; Green, K.; Williams, D.; Bainbridge, A.; Crane, K.; van Andel, T. H. *Science* **1979**, *203*, 1073.
(12) Short, M. B.; Baygents, J. C.; Goldstein, R. E. *Phys. Fluids* **2005**, *17*, 083101.
(13) Short, M.; Baygents, J.; Beck, J.; Stone, D.; Toomey, R.; Goldstein, R. *Phys. Rev. Lett.* **2005**, *94*, 018501.
(14) Double, D. D.; Hellawell, A.; Perry, S. J. *J. Proc. R. Soc. London, Ser. A* **1978**, *359*, 435.
(15) Mann, S. *Biomineralization: Principles and Concepts in Bioinorganic Materials Chemistry*; Oxford University Press: Oxford, U.K., 2001.
(16) Stone, D. A.; Lewellyn, B.; Baygents, J. C.; Goldstein, R. E. *Langmuir* **2005**, *21*, 10916.
(17) Stone, D. A.; Goldstein, R. E. *Proc. Natl. Acad. Sci. U.S.A.* **2004**, *101*, 11537.
(18) Russell, M. J.; Hall, A. J.; Cairns-Smith, A. G.; Braterman, P. S. *Nature* **1988**, *336*, 117.
(19) Russell, M. J.; Hall, A. J. *J. Geol. Soc. (London, U.K.)* **1997**, *154*, 377.
(20) Van Bommel, K. J. C.; Friggeri, A.; Shinkai, S. *Angew. Chem., Int. Ed.* **2003**, *42*, 980.
(21) Nakamura, H.; Matsui, Y. *J. Am. Chem. Soc.* **1995**, *117*, 2651.
(22) Nakamura, H.; Matsui, Y. *Adv. Mater.* **1995**, *7*, 871.
(23) Chaudhary, Y. S.; Ghatak, J.; Bhatta, U. M.; Khushalani, D. *J. Mater. Chem.* **2006**, *16*, 3619.
(24) Miyaji, F.; Davis, S. A.; Charmant, J. P. H.; Mann, S. *Chem. Mater.* **1999**, *11*, 3021.
(25) Ritchie, C.; Cooper, G. J. T.; Song, Y.-F.; Streb, C.; Yin, H.; Parenty, A. D. C.; MacLaren, D. A.; Cronin, L. *Nature Chem.* **2009**, *1*, 47.
(26) Cooper, G. J. T.; Cronin, L. *J. Am. Chem. Soc.* **2009**, *131*, 8368.
(27) Cartwright, J. H. E.; García-Ruiz, J. M.; Novella, M. L.; Otálora, F. *J. Colloid Interface Sci.* **2002**, *256*, 351.
(28) Pantaleone, J.; Toth, A.; Horvath, D.; Rother McMahan, J.; Smith, R.; Butki, D.; Braden, J.; Mathews, E.; Geri, H.; Maselko, J. *Phys. Rev. E* **2008**, *77*, 046207.
(29) Pantaleone, J.; Toth, A.; Horvath, D.; RoseFigura, L.; Morgan, W.; Maselko, J. *Phys. Rev. E* **2009**, *79*, 056221.
(30) Bormashenko, E.; Bormashenko, Y.; Stanevsky, O.; Pogreb, R. *Chem. Phys. Lett.* **2006**, *417*, 341.
(31) Cartwright, J. H. E.; Escribano, B.; Khokhlov, S.; Sainz-Díaz, C. I. *Phys. Chem. Chem. Phys.* **2011**, *13*, 1030.
(32) Cartwright, J. H. E.; Escribano, B.; Sainz-Díaz, C. I. *Langmuir* **2011**, *27*, 3286.
(33) Cartwright, J. H. E.; Escribano, B.; Sainz-Díaz, C. I.; Stodieck, L. S. *Langmuir* **2011**, *27*, 3294.
(34) Collins, C.; Zhou, W.; Mackay, A. L.; Klinowski, J. *Chem. Phys. Lett.* **1998**, *286*, 88.
(35) Collins, C.; Mann, G.; Hoppe, E.; Duggal, T.; Barr, T. L.; Klinowski, J. *Phys. Chem. Chem. Phys.* **1999**, *1*, 3685.
(36) Collins, C.; Mokaya, R.; Klinowski, J. *Phys. Chem. Chem. Phys.* **1999**, *1*, 4669.
(37) Thouvenel-Romans, S.; Steinbock, O. *J. Am. Chem. Soc.* **2003**, *125*, 4338.
(38) Pagano, J. J.; Bánsági, T.; Steinbock, O. *J. Phys. Chem. C* **2007**, *111*, 9324.
(39) Pagano, J. J.; Bánsági, T.; Steinbock, O. *Angew. Chem., Int. Ed.* **2008**, *47*, 9900.
(40) Thouvenel-Romans, S.; Saarloos, W.; Steinbock, O. *Europhys. Lett.* **2004**, *67*, 42.
(41) Thouvenel-Romans, S.; Pagano, J. J.; Steinbock, O. *Phys. Chem. Chem. Phys.* **2005**, *7*, 2610.
(42) Müller, I.; Strehlow, P. *Phys. Bl.* **1999**, *55*, 37.